

Competing modes of instability in an electrically driven nematic liquid crystal with a small positive dielectric anisotropy

Pramoda Kumar and K. S. Krishnamurthy*

Centre for Liquid Crystal Research, P.O. Box 1329, Jalahalli, Bangalore 560 013, India

(Received 25 November 2005; revised manuscript received 25 April 2006; published 14 September 2006)

Competing modes of electric-field-driven bifurcation have been examined in a planarly aligned nematic liquid crystal with a small positive dielectric anisotropy and large electrical conductivity. The line of bifurcation into the electroconvective state is linear in frequency not only up to the codimension-2 (C2) point but well beyond. This contrasts with the recent theoretical prediction of the absence of further bifurcations within the Freedericksz state, above the C2 frequency. Further, in the frequency regime beyond C2, within the space-filling electroconvective state, a strongly localized dynamical state (SLDS) appears at a voltage threshold which again is linear in frequency. Occurrence of the SLDS through a secondary forward bifurcation is significant in view of the reported observations on the so-called worms, an instability belonging to the SLDS, as the first form of convection seen at the primary subcritical bifurcation.

DOI: [10.1103/PhysRevE.74.031705](https://doi.org/10.1103/PhysRevE.74.031705)

PACS number(s): 61.30.Gd, 47.54.-r, 47.52.+j, 47.20.Lz

I. INTRODUCTION

Electrically driven nematic liquid crystals are known to display multifarious instabilities, both in the linear and nonlinear regimes, depending on the conditions of excitation and choice of material parameters [1–3]. For instance, a planarly aligned sample, strongly positive in dielectric anisotropy $\varepsilon_a = (\varepsilon_{\parallel} - \varepsilon_{\perp})$, where \parallel and \perp denote the directions relative to the nematic director \mathbf{n} , when acted on by a field transverse to \mathbf{n} , may undergo a purely orientational, second-order transition to a homogeneously distorted state above a voltage threshold V_F (the Freedericksz effect [1,2]). By contrast, when ε_a is slightly positive and the conductivity anisotropy $\sigma_a = (\sigma_{\parallel} - \sigma_{\perp})$ is also positive, the sample may display, above some critical ac voltage $V_C < V_F$, convective structures with spatiotemporal periodicity (the Carr-Helfrich effect [1–3]); under a static field, on the other hand, the same sample may develop a flexoelectric instability [2]. Situations involving an interplay of different bifurcation mechanisms are evidently of particular importance to pattern formation in the nonlinear regime. There have been a few significant studies conducted in this area in recent years. For instance, Delev *et al.* have reported their experimental and theoretical results concerning the crossover between flexoelectric and electroconvective distortions occurring in a homeoplanar nematic subject to a dc field [4]. Similarly, Dressel *et al.* [5] have demonstrated the coupling of homogeneous and vortex modes to generate the so-called splay and twist normal rolls. More recently, Dressel and Pesch [6] have reported their rigorous theoretical analysis of the competition between electroconvection (EC) and the Freedericksz effect (FE). In this report, we present the results of our electric field experiments on the competition between EC and FE in a nematic liquid crystal with a weakly positive ε_a and discuss some of the findings in the light of related numerical-theoretical predictions mentioned in Sec. II. In particular, the splay-roll instability and bistability between the convective and Freedericksz states predicted

to occur close to the multicritical point are observed; however, beyond this point, the stability of the homogeneous state seen in the predicted phase diagram [6] is not supported by our results. Some of our observations pertain to localized structures; we discuss these with reference to earlier experimental and theoretical findings on localized instabilities briefly surveyed in Sec. III.

II. INSTABILITY THRESHOLDS AND PREDICTED BIFURCATIONS

The Freedericksz effect is an equilibrium phase transition occurring at a threshold voltage V_F determined by the balance between elastic and dielectric torques. V_F is given in terms of the splay elastic modulus k_{11} and absolute dielectric anisotropy $\varepsilon_0 \varepsilon_a$ by $V_F = \pi \sqrt{[k_{11}/(\varepsilon_0 \varepsilon_a)]}$. On the other hand, EC is a dissipative, nonequilibrium phenomenon that relies for its occurrence primarily on the electrical conductivity anisotropy. In a planar nematic with $\mathbf{n} = (1, 0, 0)$, subject to an electric field $\mathbf{E} = (0, 0, E)$, EC occurs at a well-defined reversible voltage threshold V_C , at which the originally structureless fluid breaks up into a system of periodic rolls oriented in the sample plane, either normal to the easy axis or at an angle $(90 \pm \beta)$ with respect to it; normal rolls (NR) form above the Lifshitz frequency $f_L = \omega_L/2\pi$ and oblique rolls (OR) below it [7]. An expression for V_C based on the full three-dimensional linear stability analysis is reported in Ref. [8]. Very roughly, when $\varepsilon_a \ll 1$ and the field is static, it reduces to $V_C \approx C \sqrt{[k_{11} \sigma_{\perp}/(\sigma_a \varepsilon_0 \varepsilon_{\perp})]}$, where C is a numerical constant, usually ranging between 5 and 10, and determined by various viscosity coefficients and the wave vector components (p, q) along x and y . The ratio (V_F/V_C) can easily be made to exceed unity by choosing a small ε_a (as in this study), so that, when ω is small and the voltage is gradually raised, the initial destabilization of the rest state is through EC. However, as ω is increased, since V_C is an increasing function of ω [6] while V_F is very nearly ω -independent, there occurs a crossover between the Freedericksz and EC bifurcation lines at the codimension-2 (C2) point.

*Corresponding author. E-mail address: kristy@vsn1.net

In Ref. [6], the various linear and nonlinear phase transitions occurring near the C2 point are theoretically analyzed and the complete bifurcation diagram is drawn in the $\omega' - V$ plane for doped MBBA (4-methoxy benzylidene-4'-n-butylaniline) with $\epsilon_a = 0.1$ and $\sigma_{\perp} = 10^{-8}$ S/m; here ω' is the dimensionless frequency equal to $\omega\tau$, with the space charge relaxation time $\tau = (\epsilon_o \epsilon_{\perp}) / \sigma_{\perp}$; and V is the rms voltage of the wave form $V_t = \sqrt{2} \cdot V \sin \omega t$. In this phase diagram, covering the range of ω' from 1 to 2.1, and considered to be generic for EC instabilities in nematics with a small ϵ_a , V_C , the threshold for the normal roll state, is linear in ω' and approaches the V_F horizontal from below. For continuity reasons, a transition from the Fredericksz state to EC state in the nonlinear regime is also predicted at $V'_C > V_F > V_C$; the corresponding bifurcation line is shown to meet the C2 point ($\omega' = 1.99$) from above V_F , the two lines of bifurcation into the EC state forming a wedge nearly symmetric with respect to the horizontal at V_F . The states of OR and splay rolls (SR) belonging to the nonlinear regime occur above V_C , but below or above V_F depending on ω' . It is necessary to emphasize that the analysis in Ref. [6] is for $\omega' > \omega_L$, or for initial bifurcation into the normal ($\beta = 0$) roll state; but for lower frequencies, the first bifurcation, which is to the OR state, is predicted to occur only slightly below the normal roll threshold. Most importantly for the present study, the reported theoretical bifurcation diagram predicts no secondary instabilities within the Fredericksz state, beyond the C2 point frequency.

It is pertinent to mention here a recent experimental study [9] on the electric field-induced instabilities in a nematic azoxy mixture (Merck ZLI-3086) with $\epsilon_a \approx 0.06$ (measured) and $(\sigma_{\parallel} / \sigma_{\perp}) \approx 2.4$ (fitted), exhibiting the C2 frequency of 30 Hz. Above the C2 frequency, the system shows no evidence of EC and any domain wall formed at the transition to the Fredericksz state transforms into a pair of disclinations (pincement) at a high enough voltage. Below the C2 point, the OR state occurs at the primary bifurcation; slightly above V_F , the rolls change over to loop-walls elongated along the y direction; well above V_F , a dynamic and helixlike modulation occurs along the domain walls. This modulation has been termed the ‘‘corkscrew’’ instability and described in terms of a pitchfork bifurcation; its frequency dependence is conjectured to arise from EC. Incidentally, some early reports on BEPC in both planar and twisted geometries also mention of the possible involvement of ionic conduction in the distortion of otherwise elliptical walls formed at the Fredericksz transition (Leger-Brochard walls), and the complex wavy nature of the focal lines due to the walls, seen at higher voltages and lower frequencies [10,11].

III. STRONGLY LOCALIZED DYNAMICAL STATE

In a translationally invariant, spatially extended, driven dissipative system, periodic structures are sometimes excited only in isolated domains randomly distributed within the homogeneous quiescent state. This nonlinear nonequilibrium phenomenon is known in a great variety of physical, chemical, and biological systems [12]. Particularly significant to our present study is the localized dynamical state arising in

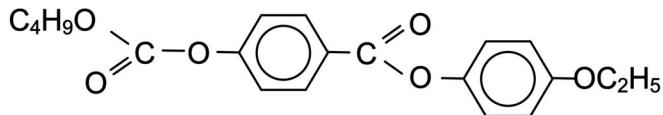
fluid media; some early examples of quasi-one-dimensional confined roll structures were realized, via a backward Hopf bifurcation, in binary-fluid Rayleigh-Benard convection in narrow channels [13]. These structures, sometimes referred to as ‘‘pulses,’’ correspond to the pulse solutions of the quintic complex Ginzburg-Landau equations (CGLE) [14]. In two-dimensional (2D) binary liquid convection, the initial linear traveling roll state, established again through a backward bifurcation, gives way in time to a confined nonlinear state; but the latter, though long-lived, proves eventually to be transitory [15]. In nematics, localization of traveling rolls, not ascribable to any finite size effect and arising through a direct bifurcation, was discovered by Joets and Ribotta [16]. They observed in nematic materials (MBBA and Merck Phase V) with positive σ_a and negative ϵ_a , under ac excitation at frequencies close to the limiting frequency of the conduction regime, isolated and nearly elliptical domains of traveling normal rolls, surrounded by the quiescent fluid; the domains, with their major axis along x , are typically of dimensions comparable to the sample thickness d ; instances are also noted, however, of domains quite elongated in the x direction, comprising rather short rolls ($1-2 d$ along y) and, in effect, forming quasi-1D (one-dimensional) traveling-wave patterns. Importantly, the localized state in Ref. [16] is not associated with any drift velocity; further, it enlarges on raising the control parameter toward the space-filling state. More recently, Dennin *et al.* [17] have observed in a nematic liquid crystal, 4-ethyl-2-fluoro-4'-[2-(trans-4-pentylcyclohexyl)-ethyl] biphenyl (I52), with $\sigma_a > 0$ and $\epsilon_a < 0$, below a critical value of (σd^2) , strongly localized structures occurring right at the primary bifurcation; these pulses, which comprise swiftly propagating oblique rolls that pass under a slowly drifting envelope, have been referred to as ‘‘worms’’ in view of their slender appearance and movement; the worm state may equally well be described as the SLDS. Later investigations have shown the bifurcation to this SLDS to be subcritical [18]; as the control parameter ϵ , defined in terms of the applied voltage V and its threshold value V_C by $\epsilon = (V^2 - V_C^2) / V_C^2$, increases towards 0 value, the SLDS gradually tends toward the space-filling OR state. Further, above a critical (σd^2) , the transition to the extended OR state occurs directly from the basic state via a supercritical bifurcation. These results obviate the existence of bistability between the basic and nonlinear states, and the stability of the SLDS, therefore, is not explicable by invoking ‘‘fronts.’’ The SLDS is thought to arise from a combination of zig and zag waves, either left traveling or right traveling. It has been shown that the usual CGLE for the oblique waves, when coupled with a weakly damped charge-carrier mode, can lead to localization while preserving the supercriticality of the transition to the extended state [19].

Localized time-dependent states have also been observed in nematic 4'-hexyloxyphenyl 4-decyloxybenzoate (10E6) [20]; they manifest as anisotropic clusters of short oblique rolls at low frequencies and flickering butterflylike objects at high frequencies; these instabilities occur in the vicinity of the smectic-nematic transition temperature where σ_a turns negative and $\epsilon_a < \sigma_a < 0$; in this situation, since the Carr-Helfrich mechanism breaks down, these localized states do not conform to the standard model.

We have observed some strongly localized dynamical structures which, besides having a distinctive morphology, occur only after the onset of the Fredericksz state. Their features are discussed in Sec. V B

IV. EXPERIMENTAL DETAILS

We used a reagent grade sample of butyl 4-(4-ethoxyphenoxy) carbonyl phenyl carbonate (BEPC),



supplied by Eastman Organic Chemicals. It exhibited an enantiotropic nematic phase between approximately 55 °C and 84 °C. The sample cells were sandwich type, constructed of glass plates coated with indium tin oxide (ITO). Mylar spacers, heat sealed to the electrodes through cooling from approximately 250 °C under a uniform pressure, determined the cell spacing, d . The d value was determined interferometrically, using channeled spectrum. For securing a planar alignment of the samples, the electrodes were rubbed unidirectionally on silk prior to cell construction and no surfactant material was used. We take the easy direction and the layer normal to define the reference axes x and z , respectively. Observations were carried out in transmitted light, along z , using a Leitz DMRXP polarizing microscope, equipped with a Sony charge-coupled device (CCD) camera and a Mettler FP90 hot stage. The electric field was applied along $\pm z$. The voltage source was a Stanford Research Systems DS 345 function generator coupled to a FLC Electronics voltage amplifier (Model F20ADI). The applied voltage, V , was measured with a HP 34401A multimeter.

The value of ϵ_a for BEPC is reported to vary from 0.21 at the melting temperature to 0.06 at 84 °C [21]. The results of our independent dielectric measurements on BEPC agreed with the reported data to within 5%. For fresh samples of BEPC, σ_{\perp} varied between 6.85×10^{-8} S/m at 55 °C and 19.25×10^{-8} S/m at 75 °C; also, $\sigma_{\parallel}/\sigma_{\perp}$ decreased from 1.25 at 55 °C to 1.19 at 75 °C; with prolonged use, the sample conductivity is found to increase; the σ values given here apply through out except where stated otherwise. The birefringence of BEPC is reported to range from 0.141 at 56 °C to 0.087 at 83 °C [22].

For convenience, when the polarizer has its transmission axis along x and the analyzer along y , it will be represented as $P(x)$ - $A(y)$; $P(45)$ - $A(135)$ indicates diagonal setting of polarizer and analyzer, with the angles in parentheses in degrees measured from the x direction.

V. EXPERIMENTAL OBSERVATIONS AND DISCUSSION

A. Instabilities below the C2 frequency

Figure 1 shows the experimental phase diagram for BEPC up to the C2 point corresponding to 75 °C. Before discussing it, a point of clarification is in order. V_C is the optical threshold at which the EC roll pattern appears; it is expected to be slightly higher than the true threshold. Likewise,

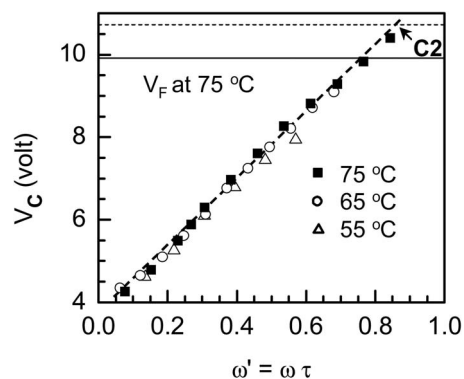


FIG. 1. The threshold voltage for electroconvection V_C as a function of the dimensionless frequency $\omega' = \omega\tau$. The dotted horizontal line at 10.7 V is the optical Fredericksz threshold V_F at 75 °C; the continuous horizontal line gives $V_F = 9.8$ V at 75 °C from cell capacitance data. The codimensional-2 point (C2) is indicated only for 75 °C, the temperature at which the instabilities beyond C2 were investigated (see text). The C2 value decreases with temperature.

$V_F (=10.7$ V at 75 °C) is the optical threshold corresponding to the onset of a change in birefringence color; relatively, V_F from capacitance measurements at 1 kHz is found to be $\sim 9\%$ lower (Fig. 2). Thus the C2 frequency ω'_{C2} of 0.86 (corresponding to 560 Hz, with $\tau = 0.24$ ms) is approximate to the extent the two optical thresholds differ in the degree of their overestimation.

As depicted in Fig. 1, V_C is linear in ω' at any given temperature. While this is only to be expected in the high frequency region ($\omega' > 0.7$ for doped MBBA [6]), a nonlinear scaling of V_C , roughly as $\sqrt{1 + \omega'^2}$ when $\epsilon_a \ll 1$, is predicted at lower frequencies [6,8,23]. In other words, $V_C - \omega'$ curve should have a zero slope at the low frequency limit. Thus the behavior observed in the low frequency region tantamounts to a depression of the threshold from its theoretical value by a quantity that decreases continuously with increasing frequency. This could come about from flexoelectric influence at least at very low frequencies, particularly in thin samples [23]. In fact, for a static field acting on an initially planar sample, theoretical finding is that flexoelectric effect reduces the EC threshold (e.g., Ref. [4] and references therein). For ac fields, the flexoelectric influence

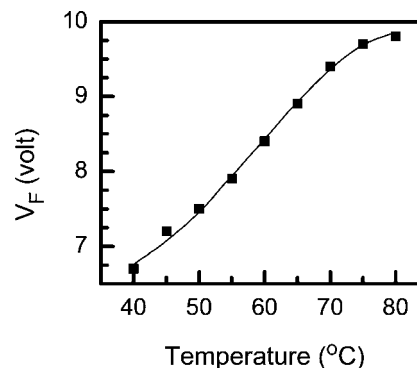


FIG. 2. Fredericksz threshold V_F from cell capacitance measurements as a function of temperature.

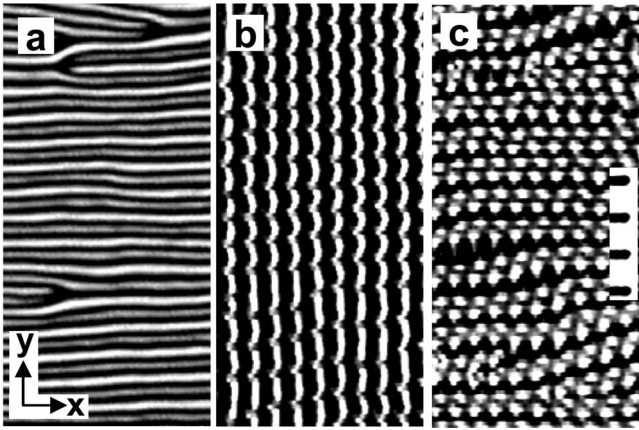


FIG. 3. Contrast enhanced, gray scale reproduction of the patterns observed in a $4.65 \mu\text{m}$ thick sample under low frequency driving at 75°C and 6.73 V . (a) 1 Hz , $P(x)-A(y)$; (b) and (c) 15 Hz , $P(x)-A(x)$; the snapshots in (b) and (c) are recorded at different times during the variation in the instantaneous voltage of the applied wave form. Each scale division in (c) corresponds to $10 \mu\text{m}$.

is likely to decrease progressively with increasing frequency. In fact, in BEPC subject to a static or very low frequency field, we do observe the Bobylev-Pikin domains [2] characterized by a pattern of stripes, periodic in y and parallel to the easy axis, as in Fig. 3(a); this is a nonconvective instability involving periodic (θ, φ) variations defined by $\theta = \theta_0 \cos(qy) \cos(\pi z/d)$ and $\varphi = \varphi_0 \sin(qy) \cos(\pi z/d)$, where q is related to the spatial frequency or domain density ν by $q = \pi\nu$. On the other hand, above approximately 25 Hz , at a well-defined voltage threshold, the sample displays EC in the form of oblique rolls that tend to align normal to the easy axis with progressive voltage elevation. We present in Fig. 3(b) what is predominantly a pattern of normal stripes obtained with a frequency of 15 Hz and control parameter, $\varepsilon = 0.96$; the bright vertical stripes in the figure display an intensity modulation almost periodic in y ; this feature is similar to the one reported in Ref. [4] as illustrating the competition between stationary flexodomains and drifting EC rolls. In fact, for the field parameters in Fig. 3(b), the pattern continuously changes with the instantaneous voltage; Fig. 3(c), which is another snapshot illustrating this change, shows the stripes extended mainly along x . Above 20 Hz , flexoelectric contribution to distortion is difficult discern in optical textures.

The initial EC pattern for a frequency above $\sim 20 \text{ Hz}$ is that of OR for the entire frequency range up to the C2 point so that $\omega'_{C2} < \omega_L$. In Fig. 4(a), we present a typical texture observed in the low frequency region at $\varepsilon = 0.4$, under parallel illumination of the sample with white light polarized along the easy axis. The microscope is focused to display the real images. The focalization of light seen in the figure is primarily due to the periodic out-of-plane director deviations θ that lead to an undulation of the extraordinary planar wave surface incident on the sample [24]; expectedly, focusing action disappears for incident light vibrating along y . The zig and zag regions, which are similar in appearance, display an alternation in the sharpness of focal lines; this feature, com-

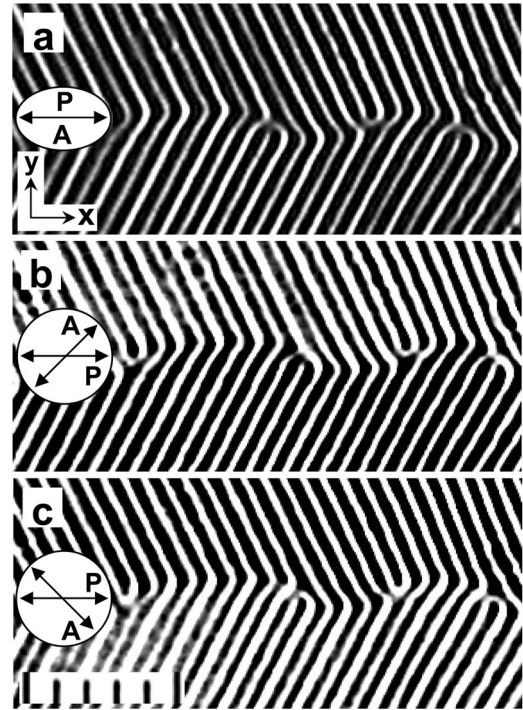


FIG. 4. Gray scale images of the zig-zag roll pattern observed in the same sample region for $\varepsilon = 0.4$, 70 Hz , $d = 6.3 \mu\text{m}$, and 75°C . (a) Bright lines are the focal images in the real plane, formed due to a periodic director deviation along x ; they appear with maximum contrast in extraordinary light showing that the focusing is due to deviations θ in the xz plane. Alternate lines are focused in two different xy planes, causing the sharpness change between successive lines; $P(x)-A(x)$. (b) The contrast between the zig and zag zones is due to the opposite azimuthal tilts in these zones; $P(x)-A(45)$. (c) The contrast in (b) is reversed with the analyzer turned to -45° position. Each division in the scale is $10 \mu\text{m}$.

monly found for the roll pattern and first noticed by Penz [25], was later explained by Kondo *et al.* [26] who considered, along with the wave surface distortion, the deflection of the extraordinary ray from the wave normal. A more profound analysis of the emergent optical field is due to Joets *et al.* [27] who invoke the Curie principle to relate it with the symmetry of the nematic director field. They demonstrate that when light vibrating along x is incident perpendicularly on a nematic layer in the normal roll state, the emergent nonparallel rays generate an array of cusped caustics, with the cusp lines along y . For real caustics, these lines occur alternately on two different $z = \text{constant}$ planes, with a constant periodicity along x (see Fig. 10 discussed later). This indeed is the underlying reason for the difference in focus between the alternate bright lines in Fig. 4(a).

The snapshot in Fig. 4(b), obtained with the configuration $P(x)-A(45)$, and corresponding to the same region of the sample as Fig. 4(a), displays a difference in the gray scales between the zig and zag regions. Before discussing this aspect, we note that the birefringence and the thickness are both low for our samples; as a result, the Mauguin waveguide condition [28] does not quite apply here and an in-plane director deviation reveals itself between suitably oriented polarizers. More specifically, the Mauguin regime is

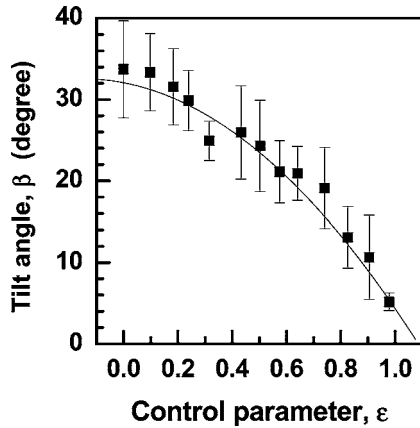


FIG. 5. Tilt angle β of the oblique rolls with respect to the y axis as a function of the control parameter; the curve represents the second-order polynomial fit; 75 °C, 30 Hz.

governed by the condition $(n_e - n_o)p \gg \lambda$, with n_e and n_o denoting the extraordinary and ordinary refractive indices, p the pitch of the helical structure, and λ the wavelength. For BEPC, $(n_e - n_o)$ at 75 °C is ~ 0.11 [22]. If the azimuthal deviation in the sample midplane ($z=0$ plane) is taken for argument as 25° , the effective pitch is $7.2d$ or $\sim 43 \mu\text{m}$ for a $6 \mu\text{m}$ thick sample. Correspondingly, the ratio $(n_e - n_o)p/\lambda$ varies between 6 and 11 for different wavelengths in the visible range. With the distortion also involving a polar deviation θ , the effective birefringence becomes less than $(n_e - n_o)$. When the path difference corresponding to the pitch is four to five times the wavelength, the departure from adiabatic approximation reveals itself in the transmitted light (e.g., Ref. [29]). Thus the difference in gray scales between the zig and zag regions in Fig. 4(b) indicates the presence of an azimuthal (φ) deviation of the director; the pattern of colors in the original image differs for the two regions, but is homogeneous in each of them; φ , which is of opposite sign for the two regions, is therefore uniform in any given xy plane in each of the regions. The y component of the director, n_y , is evidently maximum in the $z=0$ midplane and decreases to 0 at $z=\pm d/2$. Incidentally, in Fig. 4(b) (as also in Fig. 7 to follow) the bright lines in the zig and zag regions appear unequally focused, but this is not an indication of any symmetry breaking between the two regions. In fact, the contrast between the zig and zag regions in Fig. 4(b) is reversed when, keeping the focus of the microscope unchanged, the analyzer position is switched to $A(-45)$, as revealed in Fig. 4(c). The relative brightness of lines in the two OR regions is governed by the disposition of the analyzer axis with respect to the major axis of the elliptically polarized light that is generally incident on it. Since φ is of opposite sign for the zig and zag, it is possible to set the analyzer so that transmission is favored more for one zone than for the other. Also color dispersion is an important factor in determining the contrast between the zig and zag zones.

As expected [23], with a gradual increase in ε at a fixed ω , the obliqueness of the rolls decreases continuously as in Fig. 5; similarly the threshold obliqueness reduces with increasing ω , as in Fig. 6. However, the azimuthal deviation remains even when the rolls become normal so that, between

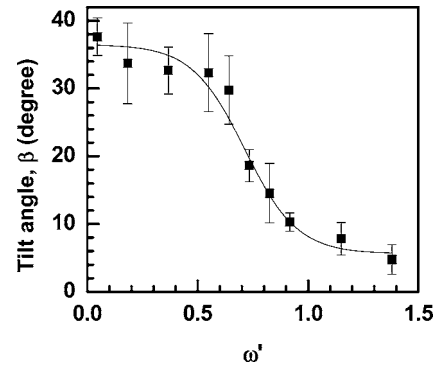


FIG. 6. Threshold tilt angle β of the oblique rolls with respect to the y axis as a function of frequency; 75 °C.

two contiguous normal roll regions with opposite φ , a demarcation boundary is formed as in Fig. 7. This is a characteristic of the so-called abnormal rolls (AR) which lack the reflection symmetry y to $-y$, just as the OR [30]. Interestingly, the AR state is not obtained in Ref. [6] for the case of threshold NR bifurcation.

To determine the bifurcations above the V_C line, we examined the instabilities after every 50 Hz, from 50 Hz to 550 Hz (ω' between 0.077 and 0.843), by gradually increasing the voltage from 0 to 22 V at each frequency. We found, with rising control parameter, the usual sequence of bifurcations into various homogeneously ordered structures of the conduction regime: OR \rightarrow AR \rightarrow bimodal \rightarrow quasiturbulence [30,31]. We could not detect the V'_C bifurcation mentioned in Sec. II, except close to the C2 point, since the sample did not completely transform to the Freedericksz state at any of the frequencies up to 400 Hz. On the other hand, above V_F , there was in general a coexistence of the convective and homogeneous instabilities. This result is in consonance with the phase diagram of Dressel and Pesch [6], who emphasize that the V'_C line has no relevance in

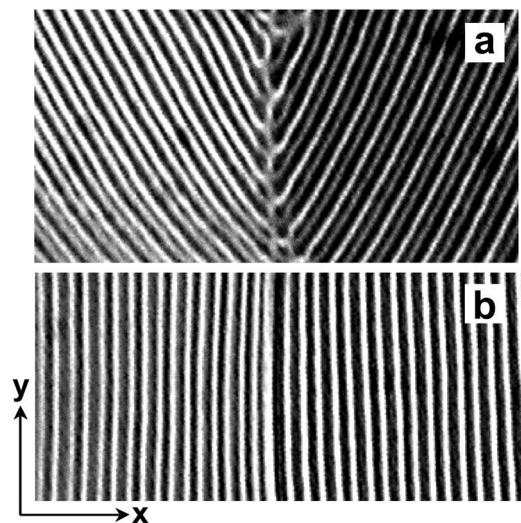


FIG. 7. (a) Vertical domain boundary between zig and zag regions near threshold. (b) Normal rolls derived from the oblique rolls well above threshold; partially crossed polarizers; $d=5.95 \mu\text{m}$, 75 °C.

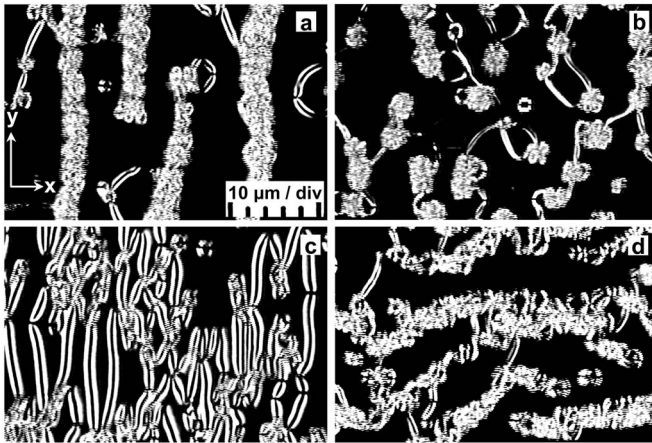


FIG. 8. Patterns due to competing electroconvective and Fredericksz reorientational modes; $P(x)-A(y)$, 75°C , $d=4.6\ \mu\text{m}$. (a) Dark background corresponds to homogeneously oriented region and the bright, broad bands, predominantly along y , represent the quasiturbulent, electroconvective regions; narrow bands of a pair of bright lines are walls in the Fredericksz state; 150 Hz, 16.34 V. (b) Tendency of turbulent zones to break up into small, circular clusters with increasing V and ω ; 300 Hz, 21.9 V. (c) Many walls in the Fredericksz state with marginal turbulence; 400 Hz, 13.5 V. (d) Increased turbulence at 20.3 V, 400 Hz, showing as irregular bright bands stretched mainly along x .

principle when the voltage is increased from below; they find convective Galerkin solutions far above the line in the non-linear regime. They also state that, except close to C2, bistability exists above the V'_C line between the Fredericksz and convective solutions. Only very close to C2 (within ~ 0.1 of ω'_{C2}), the convection is predicted to cease altogether, at a voltage V_{F2} occurring above V'_C , with $(V_{F2}-V'_C)$ approaching nonlinearly the 0 value at C2.

Figure 8 shows some of the typical textures that illustrate the coexistence of quasiturbulent and homogeneous zones above V_F . In Fig. 8(a), the uniformly dark zones represent the Fredericksz state, and the broad bright bands, the weakly turbulent state evolved through the well-established sequence of convective structures [31], starting with the OR instability. The bright bands occur randomly and irregularly; with efflux of time, they subside and give way to homogeneous reorientation in one location, but will reappear in another. They seem to comprise collapsing and evolving loop-walls, disclinations and oscillatory structures that cause spatiotemporal fluctuations in the distortion amplitude.

From the large area of the dark zones in Fig. 8(a), one might conjecture a further expansion of the Fredericksz state at higher voltages. To verify this aspect, we separately examined the sample right up to the cell breakdown voltage (~ 40 V) at 150 Hz, but found EC to exist ceaselessly throughout. In fact, the zones of turbulence become more prominent at elevated voltages, particularly at lower frequencies. Second, the bands of weak turbulence, which appear extended in the y direction at lower frequencies, tend to form in the x direction at higher frequencies. This, in turn, reflects the tendency of the rolls to transform to loop-walls extending along y or x depending, respectively, on whether EC is more

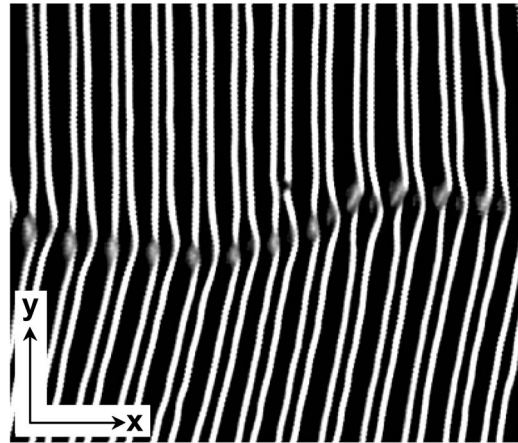


FIG. 9. Splay rolls observed close to the C2 frequency; the zig and zag rolls are nondegenerate (oriented at different angles with respect to y), with the rolls in the upper half being nearly normal; $P(x)-A(x)$, 11.1 V, 500 Hz, $d=4.6\ \mu\text{m}$.

dominant than FE or vice versa. These walls [see Fig. 8(c), for example] are more complex than the usual Leger-Brochard walls [1] which involve mainly the polar angle deviations of \mathbf{n} ; here, significant in-plane deviations are evident from the pairs of bright lines seen for $P(x)-A(y)$. The wall structure undergoes frequency-dependent complex changes at higher fields [10]; more importantly, in the high field regime, as demonstrated in Ref. [9], the corkscrewlike focal line formed in the wall region drifts continuously, revealing the presence of fluid motion within the walls; these features have been attributed to electroconvection associated with the wall state.

It is predicted in Ref. [6] that, in the vicinity of the C2 point, the splay rolls appear after the onset of FE. This is confirmed in our experiments. We found SR first at about 400 Hz, corresponding to $\omega' \approx 0.6$. In Fig. 9 showing the SR texture, the bright lines are the focal images in the real plane. The spacing between successive lines repeats alternately, which is to be expected when the homogeneous splay and periodic EC modes are coupled. At this point, an important question arises as to whether the pairing of focal lines might not be due to other causes. It is again necessary here to draw attention to Ref. [27] wherein the emergent optical field for an electroconvecting nematic is extensively analyzed and the pairing of focal lines (cusp lines) is shown to occur under different circumstances. To appreciate this, consider Fig. 10, which is based on the optical imaging model in Ref. [27] for the normal rolls. It shows the equidistant real and paired virtual cusps in the EC mode; this is explained by considering the two symmetry elements of the periodic distortion mode, namely the vertical mirror and the binary axis along z , both located centrally between adjacent rolls. They enforce corresponding symmetries in the real caustics and lead to equally spaced succession of real cusps along x . For OR, under normal illumination, significantly the same results hold since, in this case, even though the mirror symmetry is lost, the rotation symmetry is still preserved. It is only when the incident light rays are confined to yz plane, but inclined to z , both the symmetries are broken in the OR state (as also

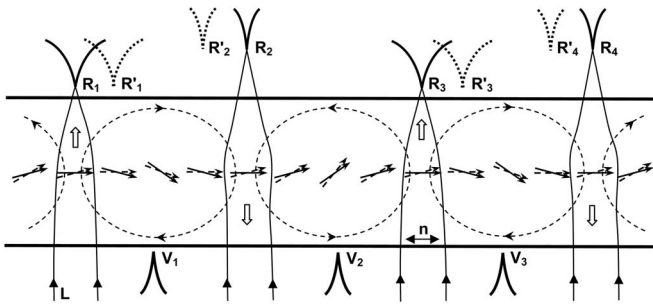


FIG. 10. Schematic of the effect of coupling between periodic and homogeneous splay modes, based on the optical imaging model in Ref. [27]. The nematic slab with its easy axis \mathbf{n} along x is confined between the thick horizontal lines. Parallel beam of light (L) is incident along z , from below. Fluid flow is indicated by broken elliptical lines and the block arrows; row of continuous-line arrows in the sample midregion represents the director field appropriate to the periodic mode; row of broken-line arrows in the midregion represents the director field in the coupled mode; R and V denote real and virtual cusps formed under the periodic EC mode; R' denotes the real cusps for the coupled mode. The pairing of real lines under parallel light illumination indicates the presence of coupled FE and EC in both NR and OR states (see text).

in the AR state), leading to a pairing of real lines. Following this line of reasoning, we may conclude that the pairing of real cusps under parallel light illumination as indicated in Fig. 9 is compatible with a coupling between homogeneous splay and periodic EC distortions under which both the reflection and binary rotation symmetries of the structure are lost.

B. Instabilities beyond the C2 frequency

According to the standard-model-based linear stability analysis [23,32], the Freedericksz state derived at the primary bifurcation remains stable against EC for any voltage above V_F , in the frequency limit $\omega \rightarrow 0$. Essentially, the reasoning here is that the destabilization effect of the Carr-Helfrich term reduces with the increasing director tilt accompanying the voltage rise above V_F ; in fact, at a large enough voltage (or angle of tilt), this term starts exercising a stabilizing influence; in effect, as V increases, V_C shifts further and further above the set voltage. The theoretical-numerical analysis in Ref. [6] shows the Freedericksz solution as unique even at higher frequencies, beyond the C2 point. In BEPC, contrary to this prediction, we find that the Freedericksz state, obtained directly from the base state at V_F , gets destabilized at a sufficiently high voltage. Figure 11 shows the secondary bifurcation threshold to lie on the V_C transition line extended from region A into region B, indicating that the origin of the new instability is again EC. In Fig. 12(a), we present the texture observed slightly above the C2 frequency, at 600 Hz. It shows the coexistence of the OR state with the evolving NR state. The two instabilities are dynamic and the initial large inclination β of the OR tends to reduce with time. With further increase in V , the oblique rolls become less inclined to y and transform into vertically extended loops; in Fig. 12(b), showing this aspect, diagonal arrays of

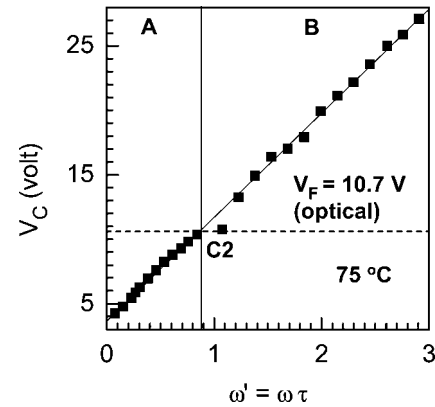


FIG. 11. Destabilization of the Freedericksz state by electroconvection beyond the C2 point (region B). Region A below C2, included for comparison, is discussed in Sec. IV A.

elliptical walls left behind by the receding OR boundary are also seen. Significantly, the real and virtual focal planes of the normal stripe state to which Figs. 12(b) and 12(c) refer are separated by as much as $\sim 80 \mu\text{m} = 14d$. This may be compared with the threshold focal plane separation of about $5d$ for the usual oblique roll pattern [24,25]. The low focal power found here implies a small amplitude of the periodic θ distortion that is superimposed on the homogeneous splay due to the FE. Figure 12(d) shows the gray scales image of the two phase pattern as observed between nearly crossed polarizers with a quarter-wave plate. Here the contrast in shade between the zig and zag zones arises from the opposite azimuthal tilts in these two regions; the normal stripe re-

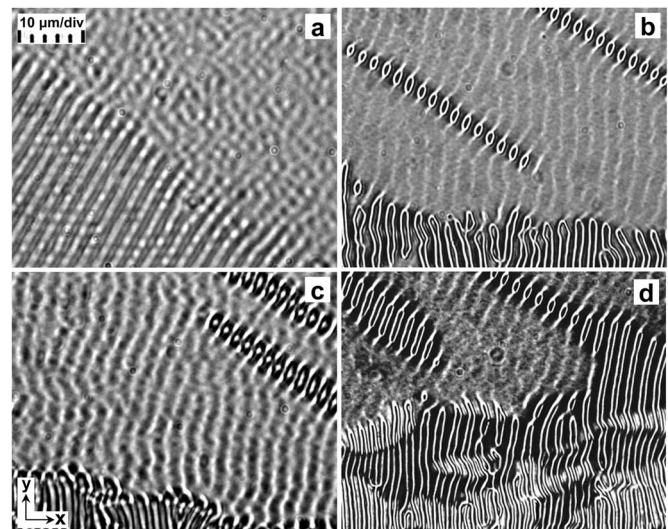


FIG. 12. Instabilities just beyond the C2 point; 600 Hz, 74°C , $d = 5.9 \mu\text{m}$. (a) Oblique rolls formed below the diagonal from top-left to bottom-right corner, coexist dynamically with evolving normal rolls above the diagonal; 10.69 V, $P(x)-A(x)$. (b) Zig-zag stripes with reduced β and more pronounced normal stripes in the real focal plane (of normal stripes) at 11.93 V; $P(x)-A(x)$. (c) Same as (b), but for virtual plane in focus. (d) conditions as in (b) but for $P(x)-A(78)$ with $\lambda/4$ plate. In the lower part of (d), the darker background of zags (///) compared to the zigs (\\) arises from the opposite azimuthal tilts of the two regions.

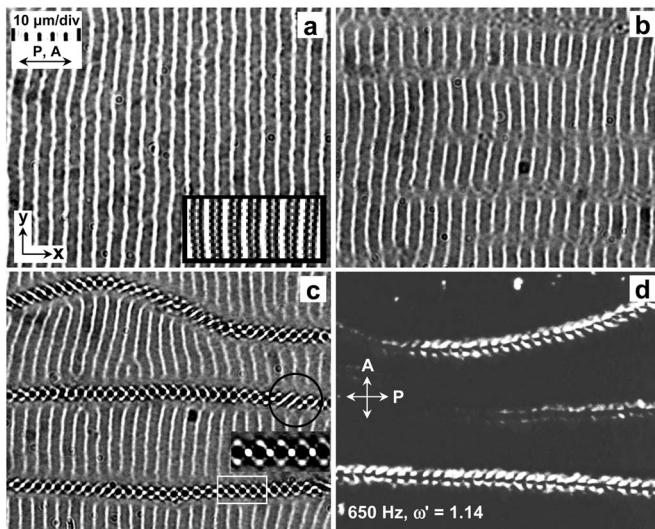


FIG. 13. Contrast enhanced, gray-level textures typical of instabilities observed in a $5.9 \mu\text{m}$ thick sample, above V_F at 650 Hz. (a) Normal stripes; 14.46 V; inset, from a $8.5 \mu\text{m}$ thick sample, clearly shows the presence of weaker focal lines alternating with stronger lines. (b) Incipient strongly localized dynamical state (ISLDS) developing along horizontal bands dividing the NR region. (c) SLDS occurring in narrow horizontal bands; 15.77 V; well-defined zags seen inside the dark circle are an indication that oblique rolls make up the localized structure; the inset is an enlargement of the localized structure inside the rectangle (in white) showing a square grid-like pattern. (d) Appearance of SLD structures between crossed polarizers; 15.77 V.

gions, on the other hand, appear with the same color, indicating the possible absence of φ . Further, the NR pattern exhibits maximum contrast for the light vibrating along x (the extraordinary vibration) and vanishes for the electric vector along y . This optical behavior is similar to that of the usual normal and oblique roll patterns at threshold and provides the necessary evidence for the existence of a periodic splay-bend distortion in the xz plane, as noted very early in the literature [24]. Should a y component of the director be present at all, it would not be accompanied by a z component in the absence of focalization of light vibrating along y .

For $\omega' = 1$, at the secondary bifurcation, the pattern of NR presented in Fig. 13(a) is obtained. Incidentally, the reason for describing the instability here as that of NR is because of the disposition of the focal lines predominantly along the y direction; however, as a careful examination of the figure would reveal, these lines possess a beaded appearance, as though they are composed of very short and irregularly spaced zigs and zags. This is a feature not observed with the usual NR pattern in thick samples. Above 650 Hz ($\omega' = 1$), only the normal stripe texture appears at the onset of EC, and the OR state is not seen. It appears, therefore, that the Lifshitz frequency f_L separating the threshold NR and OR states is around 600 Hz for the samples investigated.

Could the normal stripe instability be simply a static periodic modulation within the Freedericksz state rather than EC? Periodic deformations are known to exist within the Freedericksz state of some electrically driven nematics [33], but their occurrence is confined to the frequency region in

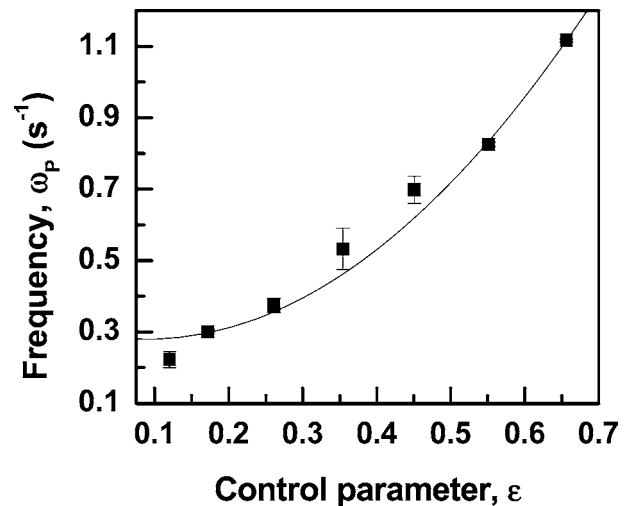


FIG. 14. Propagation frequency ω_p of the normal rolls as in Fig. 13(a) as a function of control parameter. The curve represents the second-order polynomial fit; 75°C .

the neighborhood of ϵ_a sign reversal and they are not associated with any velocity field. For BEPC, on the other hand, the dielectric relaxation frequency is 0.4 MHz at 60°C [21]; and, more importantly, the periodic instability in question, is associated with cellular flows as evident from our observation in a thicker sample ($d = 8.5 \mu\text{m}$) of the apparent oscillatory motion of suspended dust particles orbiting about the roll axes.

The periodicity of the bright stripes in Fig. 13(a) might appear at first glance to be double that expected for the usual normal rolls. But, on close inspection it may be seen that a much weaker focal line exists between successive intense lines; in other words, here too the periodicity λ of the rolls is about $2d$. This fact is clearly demonstrated in the inset of Fig. 13(a), showing the corresponding pattern obtained with a thicker sample ($d = 8.5 \mu\text{m}$). Another corroborative EC feature observed in the NR state concerns the phase propagation within the periodic structure, along the easy axis; a plot of propagation frequency ω_p as a function of the control parameter ϵ is shown in Fig. 14.

In Fig. 15 we present a plot of the critical wave number q_c in units of (π/d) as a function of the dimensionless frequency ω' , for two different conductivities. The data show a similar trend in both the cases; after a weak maximum in the low frequency region, q_c shows a slight jump near ω_L and increases nonlinearly thereafter. We may recall here that the dependence of q_c on ω' is, according to the standard model, determined by the relative signs of ϵ_a and σ_a ; when both are positive, after an initial slight rise, q_c is expected to decrease continuously with increasing ω [6]; although the low frequency behavior in Fig. 15 agrees with this prediction, beyond ω_L , q_c increases monotonically as in nematics with $\sigma_a > 0$ and $\epsilon_a < 0$ [23].

The NR state is destabilized above a voltage V_2 which again is a linear function of ω' , as shown in Fig. 16. The new instability, which may be designated as the incipient strongly localized dynamical state (ISLDS), appears in irregularly spaced horizontal bands presenting a nearly uniform aspect,

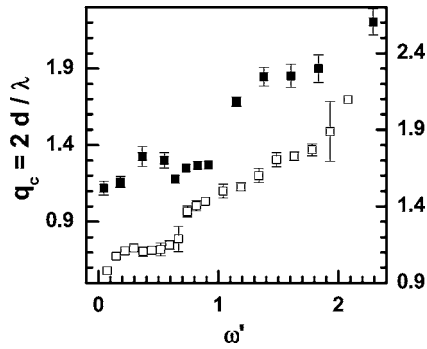


FIG. 15. Critical wave number q_c of rolls in units of π/d as a function of the dimensionless frequency ω' ; 75 °C. Filled squares are for a sample with $\sigma_{\perp} \approx 2 \times 10^{-7}$ S/m and unfilled squares are for $\sigma_{\perp} \approx 3 \times 10^{-7}$ S/m; left and right ordinates correspond respectively to filled and unfilled squares.

with the normal stripe texture completely suppressed within them, as in Fig. 13(b). In repeated experiments, these bands generally form in different unpredictable locations. With further voltage elevation, bifurcation of the ISLDS into the SLDS occurs at a threshold V_3 , which is also linear in ω' as depicted in Fig. 16. We present in Fig. 13(c) a pattern of normal stripes and SLD structures coexisting at V_3 . Here the SLD structures are, along the y direction, almost maximally and uniformly confined to a width equal to about the period λ of the normal stripes ($=10 \mu\text{m} \approx 1.7d$). But, along the easy axis, they are quite long, stretching beyond the limits of the visual field spanning over 25λ .

The localized structures in BEPC differ from the worms in I52 [17] in several significant ways.

(1) A unique feature of the pulses in I52 is their occurrence as the first form of convection, through a subcritical bifurcation; but the pulses in BEPC are obtained via a secondary bifurcation of the coupled NR and Fredericksz states; also, we find this transition to be nonhysteretic to within about 0.5 V.

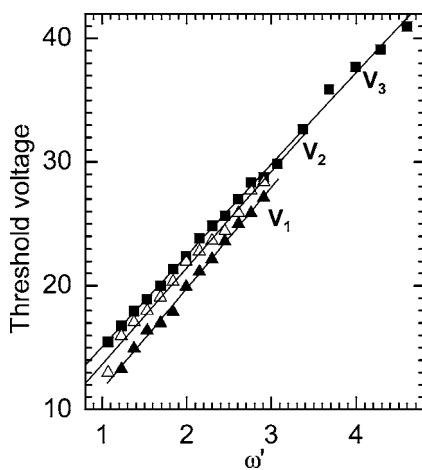


FIG. 16. Bifurcations following the transition to the Fredericksz state. V_1 is the same as V_C in Fig. 11, corresponding to the transition from the Fredericksz to the EC state. V_2 is the threshold at which EC is suppressed along horizontal bands (incipient strongly localized dynamical state, ISLDS); V_3 is the threshold of bifurcation into the SLDS.

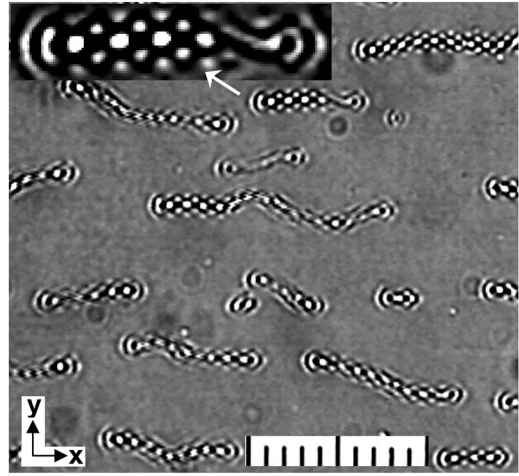


FIG. 17. Coexisting localized structures of varying length (along x) and nearly constant width (along y) at 18.9 V and $\omega' = 1.19$; 75 °C, 10 μm scale division, $P(x) \sim A(x)$, $d = 4.7 \mu\text{m}$. The inset is an enlarged image of the pulse indicated by the arrow, showing its quasi-1D hexagonal gridlike structure.

(2) The pulse state in I52, with increasing control parameter, transforms into the extended OR state via a supercritical bifurcation; but in BEPC, it goes over progressively to a quasi-turbulent state, as described in detail later.

(3) The pulses in I52 always drift backwards, i.e., in a direction opposite to that of phase propagation of the underlying roll structure; whereas in BEPC both forward and backward drifting localized domains are found. It may be recalled here that, in binary liquid convection in annular cells, both positive and negative drift velocities are encountered depending on the pulse length, Rayleigh number, and separating ratio (see, e.g., Kolodner [13(c)]); the observed interrelation between drift dynamics, pulse-length, and pulse-stability have been largely explained on the basis of extended Ginzburg-Landau equations, by considering the interaction between fronts arising from both the concentration mode and dispersion [34].

(4) The drift of the pulses in I52, when present, is confined exclusively to the easy direction; on the other hand, some very short pulses in BEPC are found to possess an additional drift component along y , as will be discussed later. It may be noted here that, according to Riecke and Granzow [19], the y drift of pulses is attributable to the difference in amplitudes of the zig and zag components that enhances the advection of the charge carrier mode towards one or the other of the lateral directions.

(5) The pulses in Ref. [17] are blurred objects crossed by vertical stripes spaced some $0.6d$ apart; the SLD structures in BEPC possess a very definitive morphology that often approximates a 1D array of square or hexagonal grids, as clearly seen in the insets to Figs. 13(c) and 17. It is necessary to clarify at this point that localized structures with well-defined features, somewhat similar to ours, have also been observed in later investigations on I52; and the exact appearance of the localized structures are remarked to be in effect determined by the shadowgraphic arrangement [18]. We do find that the setting of polarizers and the plane under focus

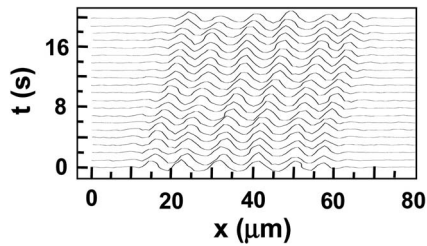


FIG. 18. Profiles of optical density along the long axis of a pulse as a function of time, extracted from the movie-mode recordings. Successive profiles are 1 s apart. The pulse drifts along x very slowly at $\sim 0.4 \mu\text{m/s}$.

(real or virtual) are among the external factors that determine the appearance of pulses.

(6) The pulses in I52 are invisible when the incident light has its vibration direction along y , implying the corresponding director distortions to be confined to the xz plane. On the other hand, the localized structures here involve both θ and φ deviations, as evident from a comparison of their aspect between parallel and crossed polarizers; focalization primarily due to periodicity in θ is revealed for parallel polarizers as in Fig. 13(c); whereas, φ variations lead to the texture as in Fig. 13(d).

There are also the following features common to the localized states in I52 [17,18] and BEPC:

(1) Pulses of widely varying lengths occur simultaneously at a given voltage as evident from the pattern in Fig. 17, and the average length of the pulses increases with the applied bias. Multiplicity of pulse lengths for the same experimental parameters is also found in binary-fluid convection and explained by the extended CGLE [34].

(2) Long localized structures drift rather slowly or do not drift at all; this again has a parallel in the dynamics of “arbitrary length” pulses of convecting binary mixtures. These pulses seem to be “self-trapped” by their own convecting concentration field; and, at their drastically reduced drift velocity, they are easily pinned down at local inhomogeneities [34]. A similar effect involving charge gradients is not unlikely in electroconvection. Even some of the short localized domains drift rather slowly as inferable from Fig. 18 or do not drift at all; standing localized structures may be qualitatively understood as due to the superposition of counter-propagating waves.

(3) Not infrequently stationary localized structures exhibit “blinking” or periodic intensity excursions occasioned by the nonlinear amplitude changes in the counterpropagating waves. In the time photographs of a localized structure shown in Fig. 19, the blinking frequency, rather intriguingly, varies for the different maxima; for the maximum indicated by the downward arrow, the frequency is about 0.25 Hz and for that indicated by the upward arrow it is about 0.5 Hz.

(4) In I52, the pulse state is found only below a critical value of (σd^2) equal to about $6 \times 10^{-18} \text{ m}/\Omega$; we have yet to ascertain if a similar critical value exists also for BEPC, but as it happens (σd^2) in our study is about $5 \times 10^{-18} \text{ m}/\Omega$ at 75°C .

In the usual bifurcation scenario for electroconvection in planar nematics with $\varepsilon_a < 0$, the NR state is first destabilized

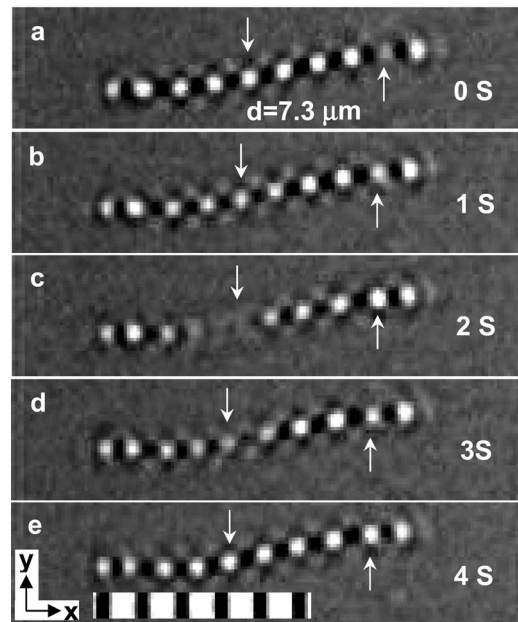


FIG. 19. Sequence of images of a localized domain taken from the movie-mode recordings at the relative times indicated, demonstrating the blinking effect. The blinking period is about 4 s at the position indicated by the downward arrow; it is ~ 2 s at the position indicated by the upward arrow. The structure is practically driftless; $10 \mu\text{m}$ scale division, 75°C .

by an undulatory modulation along the roll axis at a critical control parameter; the undulation amplitude grows with voltage to saturation and thereafter the OR state is realized [7]. This is not the sequence of events we find after the state in Fig. 13(a) is passed. Instead, the NR instability remains intact even as the OR state develops in a confined mode as in Fig. 13(c). This coexistence of the two states is somewhat reminiscent of the occurrence of an azimuthally modulated instability superimposed on the classical roll instability in MBBA with a strong initial tilt [35]. The former manifests as “extraordinary domains” (EDs) stretched along x and formed somewhat periodically along y ; each ED is composed of short oblique rolls but lined up along x . The EDs, explained as again due to the Carr-Helfrich mechanism, have also been observed in some planar samples, but as a second-order perturbation of the usual normal roll instability.

Slightly above the onset voltage of the SLDS, the normal stripes cease to exist. In fact, beyond $\omega' \approx 3$, as indicated in Fig. 16, the Fredericksz state is destabilized directly by the SLDS without the occurrence of intermediate NR and ISLD states. With continued increase in V , the SLD structures get disrupted at random locations by sudden bursts of the classic Leger-Brochard loop-wall instability. Figure 20 shows the texture obtained after the loops erupt almost at all the sites of localized structures existing at lower voltages. Eventually, the quasiturbulent state confined to some wavy bands extending along the horizontal and separating the homogeneous zones [similar to what is seen in Fig. 8(d)] is obtained. Interestingly, the EDs alluded to above are also reported to be destabilized by the turbulent state at a high enough voltage.

In the initial stages of evolution of the SLDS within the Fredericksz state, often several very short looplike pulses

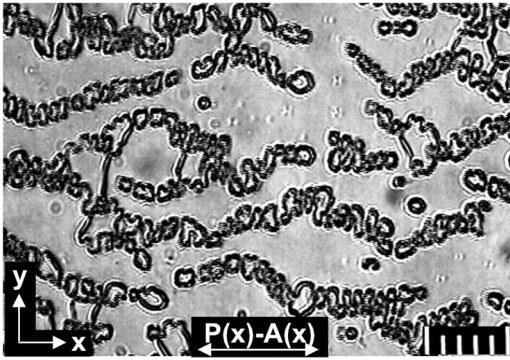


FIG. 20. Almost complete invasion of localized structures by bursting loop-walls at 20.46 V; $d=4.65 \mu\text{m}$, $\omega'=0.89$, 75°C , $10 \mu\text{m}$ scale division.

appear and this is particularly so well beyond the C2 point. Their structure, as evident from Figs. 21(a)–21(e), involves both polar and azimuthal tilts. The short pulses appearing slightly above the C2 frequency undergo rapid agitation, mostly involving oscillatory motion along x ; this is the cause of the haziness of the pulses in Figs. 21(a) and 21(b) corresponding to $\omega'=0.89$. These agitating pulses are similar to the flickering “butterflies” in Ref. [20], seen in the high frequency region in nematic 10E6 under conditions when the Carr-Helfrich mechanism is said to fail, as mentioned in Sec. III. At higher frequencies the pulses are steadier as illustrated in Figs. 21(c)–21(e). As a comparison of Figs. 21(d) and 21(e) reveals, the length of individual looplike pulses de-

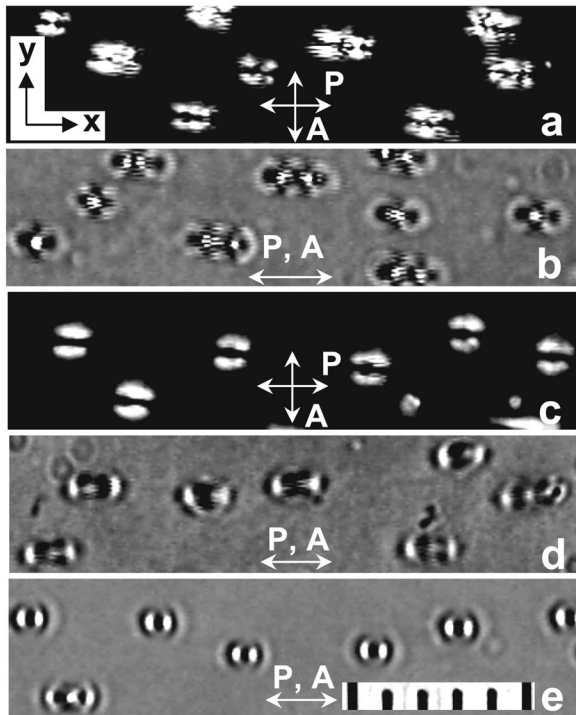


FIG. 21. Evolution of very short looplike pulses within the Freedericksz state, beyond the C2 point, in a $4.65 \mu\text{m}$ thick sample at 75°C ; $\omega'=0.89$ (a) and (b), 0.95 (c) and (d), 1.53 (e); $\varepsilon \approx 0.1$ (a)–(d), 0.7 (e). The pulses are dynamic in (a) and (b), steady in (c) to (e), and very narrow in (e), $10 \mu\text{m}$ scale division.

creases at higher frequencies and voltages. The pattern in Fig. 21(c) bears a close resemblance to the so-called beans texture reported long ago by Trufanov *et al.* [36]. Significantly, the “beans” nucleate within the Freedericksz state of an initially planar, doped sample of MBBA with a small positive ε_a ; for example, when $d=22 \mu\text{m}$, $\varepsilon_a=0.05$, $V_F=20 \text{ V}$, and $f=100 \text{ Hz}$, well before any distortion pattern is formed, electroconvection is reported to originate in thin layers next to the electrodes; corresponding dust particle rotation is found to be initially confined to the yz plane, but at a higher voltage ($=80 \text{ V}$) to the xy plane; the coherence length $\xi=(d/V)\sqrt{[k_{11}/(\varepsilon_0\varepsilon_a)]}$ at this vortex-plane switch over ($=3 \mu\text{m}$) is surmised to give the thickness of the boundary layers wherein the flows develop; importantly, the pattern of beans appears far above the convection onset, at $\sim 110 \text{ V}$. The circulations are then noticed to be around the beans formed in the boundary layers and to occur in a correlated manner with the sense of rotation reversing between the upper and lower vortices around a common axis. In an initially homeotropic sample, instead of beans, Maltese crosses are formed. These results in Ref. [36] belong to the isotropic instability mode observed in several liquid crystalline and the liquid phases. They are obviously not due to the Carr-Helfrich effect, nor are they due to the Felici charge injection mechanism [2]. They are interpreted on the basis of the electrolyte model [36] by considering the vortical currents as caused by the nonuniformity in charge distribution along z ; and the hydrodynamic instability of the director field is analyzed in terms of the velocity gradient field to arrive at the threshold behavior. We may now compare our observations relating to Fig. 21 with these results. First, in BEPC, the appearance of pulses is not preceded by development of coordinated vortical currents in the sample plane at a lower, critical voltage. Second, the motion of chance foreign particles caught in the looplike domains is often found to be oscillatory, along x ; to determine the exact nature of any convective flows associated with the short pulses, more work is needed using thicker samples where facile detection of particle motion may be possible. In any case, the coexistence of normal rolls and pulses as in Fig. 13(c), seems to suggest the involvement of conductivity anisotropy in both these instabilities such as reported in Ref. [35].

A unique feature of very short pulses in BEPC is their long-term temporal instability that becomes prominent at higher voltages. Through momentary and unpredictable oscillatory motion along the easy direction, short pulses either disappear altogether or divide to form multiple pulses. In the latter case, the site of the agitating pulse acts as a source of counterpropagating waves. Quite frequently, short drifting pulses attract one another, associate and form longer pulses. Although the drift of the short pulses is generally more pronounced along x , it may involve a smaller y component, a feature not observed in I52, as previously noted [17]. Some of these aspects are illustrated in the patterns in Figs. 22(a)–22(j), extracted from the movie-mode recordings. In Fig. 22(a), two pulses are drifting in opposite directions along x and in the same direction along y . In Fig. 22(b), “blinking” is noticed for the pulse to the right. Of the three pulses in Fig. 22(e), the top ones have drift components along $+x$ and $-y$; the lower one has the components along $-x$

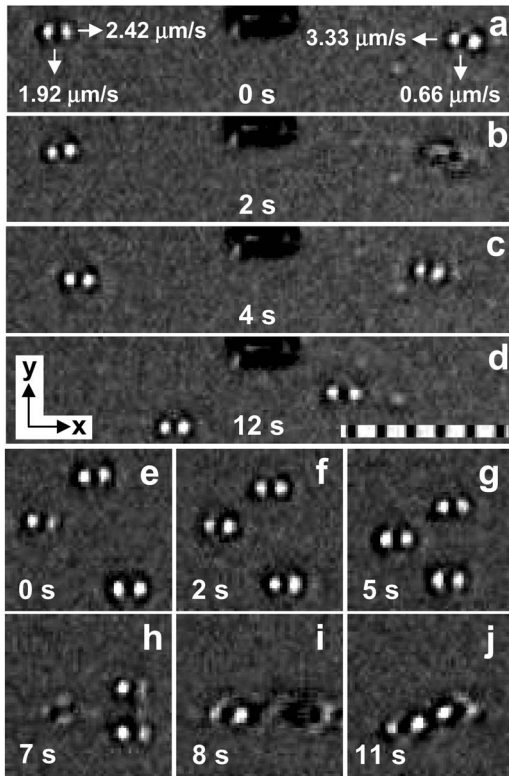


FIG. 22. Contrast-enhanced gray scales images of short pulses extracted from the movie-mode recordings revealing their drift and coupling characteristics. The large dark object at the top-center in (a)–(d) is a static impurity approached by the pulses on either side; these pulses also drift downward. The right-side pulse in (a)–(d) exhibits blinking. Images (e)–(j) show the sequence of events leading to the formation of a single bound state by three interacting pulses, 10 μm scale division.

and $+y$. The pulses eventually combine to form a single structure as in Fig. 22(j). Particulate tendency of short attracting pulses to form bound states is apparently a universal property of diverse driven dissipative systems. For instance, in binary fluid convection, Kolodner has observed that the collision between two counterpropagating pulses with a low approach velocity results in a weakly bound double-peaked structure; and Riecke has analyzed this behavior to be in agreement with the extended CGLE [37]; similarly, “oscillons” in granular media have been found, both experimentally and theoretically, to form coupled structures [38].

In Fig. 23 we present several images of localized structures observed in the real focal plane together with the intensity profiles along their long axes (usually coinciding with x). Some virtual pulse images are also reproduced in Fig. 24 for comparison. Several noteworthy aspects emerge from these patterns.

(1) The profiles in Fig. 23 display a left-right symmetry that precludes a differentiation between the pulse ends as leading and trailing edges; this contrasts with the localized structures arising from the interaction between zig and zag rolls both traveling in the same direction, $+x$ or $-x$; in that case, it is found both experimentally [17] and theoretically [19] that the roll amplitude rises steeply at one end (leading edge) and falls gradually toward the other end (trailing

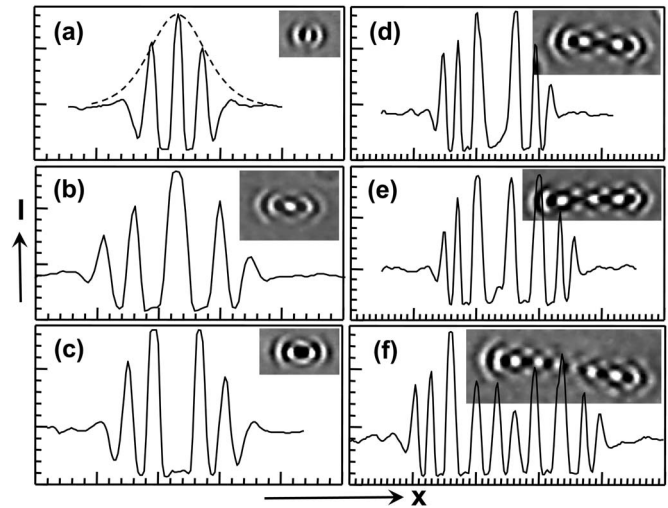


FIG. 23. Intensity profiles along the long axes of some short-length localized structures all formed at $\sim 19\text{ V}$, $\omega' = 1.25$, $d = 4.65\ \mu\text{m}$, 75°C . The insets are the real images corresponding to the profiles. Each small x division equals $2\ \mu\text{m}$; intensity I is in arbitrary units. In (a), the envelope shown by the dotted line represents $\text{sech}^2(x/\xi)$ where $\xi = 1.15d$. In (f), the drop in intensity in the middle is a blinking effect.

edge). What we probably have in Fig. 23 are the standing wave structures.

(2) The envelope of the pulse profile in Fig. 23(a) is broadly given by $\text{sech}^2(x/\xi)$ represented by the dotted curve for which $\xi = 1.15d$ (for the background-subtracted profile, we also found the same functional dependence with a marginal increase in ξ). This solitonlike property was first noted for the localized domains in Ref. [16].

(3) The pulse in Fig. 23(b) has a central principal maximum as that in Fig. 23(a), but is much longer than the latter;

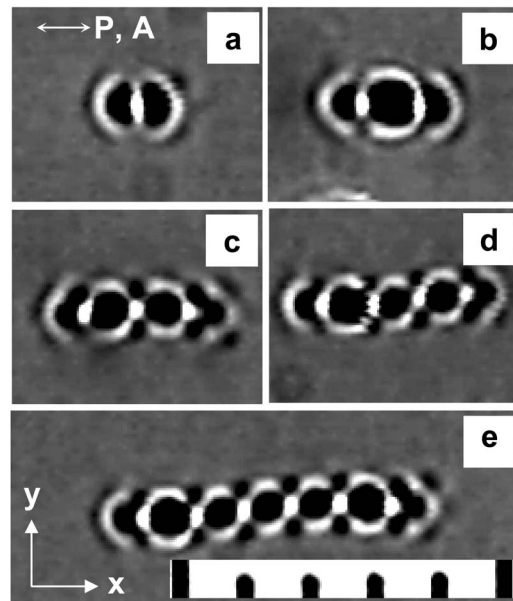


FIG. 24. Appearance in the virtual plane of some coupled pulse structures at $\sim 25\text{ V}$, $\omega' = 1.6$, $d = 4.65\ \mu\text{m}$, 75°C , 10 μm scale division.

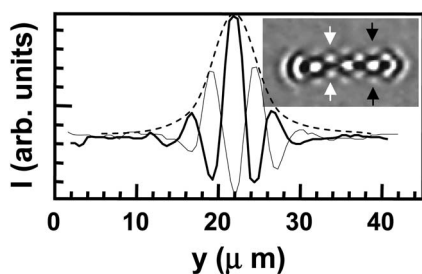


FIG. 25. Intensity profiles along y for the pulse in the inset (real image); profiles in thick and thin lines correspond respectively to the positions indicated by inverted black and white arrows in the inset. The structure is formed at ~ 19 V, $\omega' = 1.25$, $d = 4.65$ μm , 75 $^{\circ}\text{C}$. The envelope shown by the dotted line represents $\text{sech}^2(x/\eta)$ where $\eta = 0.9d$.

such an elongation is a feature usually observed before the structure dynamically passes over to the next stage of growth, as in Fig. 23(c) showing two principal maxima. Figures 23(d) and 23(e) illustrate how this process of evolution repeats itself in further growth.

(4) For the localized structures in Fig. 23, the wave number decreases from either edge toward the middle. For traveling wave pulses in binary liquid convection, the wave number is predicted [14] as well as observed [13(c)] to decrease from the trailing (upstream) to the leading (downstream) edge, sharply to begin with and slowly through the body of the pulse.

In Fig. 25 the profiles of a pulse along two different lines parallel to y are shown. Again the envelope of the peaks is solitonlike as indicated by the dotted line representing the function $\text{sech}^2(y/\eta)$, with $\eta = 0.90d$. The uniqueness of width and widely varying length that characterize the pulse state are suggestive of two separate mechanisms of confinement along and perpendicular to the pulse. Riecke and Granzow [19] consider the localized state along x to be a pair of fronts that connect “the basic state with the coexisting standing-wave-pulse state”; spatially the SLDS is homoclinic along its width, but heteroclinic along the length.

Finally, it seems relevant to mention some preliminary results relating to the appearance of the SLD state at low frequencies ascribable to the electrical history of the sample and the nature of the substrates. First, we consider the case of a thin sample, initially destabilized under dc driving by the volume flexoelectric instability; we found the (θ, φ) bands persisting, though feebly, even after several hours of turning the field off. Subsequent application of a low frequency (10–200 Hz) field induced the OR state in the sample. The rolls appearing normal to the easy axis at $\varepsilon \approx 1$ formed two sets of complementary zones of opposite azimuthal deviations. These zones with their different color patterns between suitably oriented polarizers were spectacularly dynamic and resembled the oppositely twisted zones in Ref. [39] described as associated with a breakdown of planar anchoring. More interestingly, at elevated voltages, the SLD state was realized in this sample at low frequencies as illustrated in Fig. 26. For the same parameters, pulses of varying length and area density were seen as in Figs. 26(a) and 26(b). Very long localized structures tended to be undulatory at lower

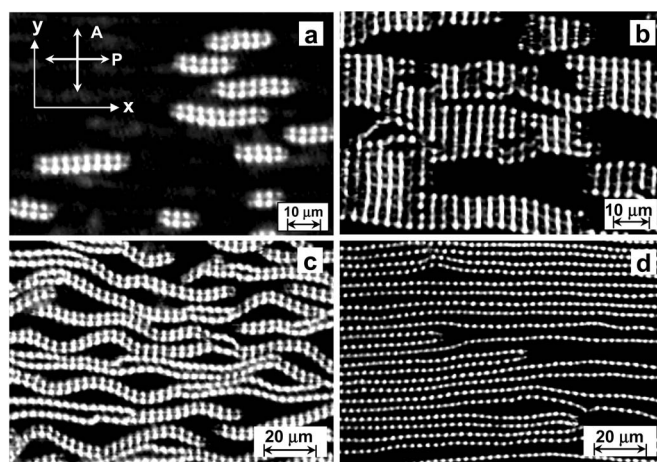


FIG. 26. SLDS at low frequencies in a 4.65 μm sample with a flexodistortion history. (a) Short pulses of varying length and (b) square grids formed of SLDS structures, in different sample regions; 62 Hz, 30.2 V, 67 $^{\circ}\text{C}$. (c) Undulatory localized structures for the same parameters as in (a), except for $f = 52$ Hz. (d) Very long and straight SLDS structures formed under high frequency excitation; keeping V at 38.6 V, frequency was decreased from 200 Hz to 91 Hz; 75 $^{\circ}\text{C}$.

frequencies, but straight at higher frequencies, as in Figs. 26(c) and 26(d). In these patterns, the pulses are seemingly a variety of oblong loop-walls maximally narrowed along y and extended to varying degrees along x ; in fact, the swift and continual surge of the bright beady images in a pulse is reminiscent of the dynamics of the corkscrew instability [9] mentioned in Sec. III.

We found another instance of low frequency SLDS in a cell constructed of plates with passivation and ITO coatings (from Delta Technology). Here, short pulses, similar to those in Fig. 21(e), appeared in horizontal chains at rather low voltages (~ 5 V) and the OR instability was not observed. This may seem to indicate the pulse state as the primary instability, bifurcating from the basic state as in Ref. [17]. However, this was not the case. As a rule, with all samples showing the low frequency pulse instability, we found a Freedericksz-type, largely homogeneous reorientation well below V_F , leading further on in voltage to pulse formation. This was readily recognized from the birefringence color change. One may tend to speculate it to be a consequence of either a pretilt occasioned by electrical history or inadequate anchoring strength or both. But we also observed the early Freedericksz-type threshold to be frequency dependent, rising from a few volts at low frequencies to the theoretical strong-anchoring, no-tilt value V_F at about 1 kHz. Strangely, this reorientation did not occur with static fields. An analogous situation is encountered in flexoelectric surface oscillations induced exclusively by ac fields, an effect observed above a frequency-dependent field threshold, at frequencies up to 30 kHz [40]. However, the amplitudes of such oscillations seem too low to produce directly observable birefringence color changes. Evidently, more work is necessary to understand the switching behavior at low voltages and pulse generation at low frequencies.

VI. CONCLUSIONS

We have reported on the interplay between equilibrium orientational and nonequilibrium convective instabilities in an electrically driven nematic liquid crystal with a small ϵ_a and large σ . The occurrence of convective instabilities beyond the codimension-2 point seems to indicate that the reported phase diagram for a relatively low conductivity nematic [6] is inadequate in describing completely the instabilities when σ is large. The OR state formed in BEPC in the low frequency regime, bifurcates into the AR state on voltage elevation. But for this behavior, the phase diagram in Ref. [6], which is in fact derived for $\omega > \omega_L$, also applies to BEPC below the C2 point. In particular, splay rolls occur close to the C2 point, as predicted. We have explored the instabilities well below the C2 frequency, up to the dielectric breakdown voltage; the Freedericksz state does not exist exclusively at any value of control parameter and bistability between the homogeneous and convective states is ever present above V_F . Our primary objective has been to highlight the existence of instabilities beyond C2 and inside the Freedericksz state. In particular, the pulse instability found in this regime at a secondary forward bifurcation contrasts with the same instability in low σ compounds, occurring as the

primary localized convective instability leading to the extended OR state [17]. The pulses in BEPC, with rising distance from their onset, are destabilized by highly dynamic loop-walls; eventually, quasiturbulent and homogeneously reoriented states coexist. In certain cases where, in the low frequency region, a Freedericksz-type effect occurs well below the V_F value corresponding to strong planar anchoring, pulses evolve within the reoriented state. This phenomenon also needs further exploration under controlled anchoring and pretilt conditions. Finally, the velocity field for the oblique convective structures, which supposedly make up the pulse state in general, is still an open question; and there seems to be no direct evidence of this field such as provided by the well-coordinated foreign particle motion attending the extended roll state.

ACKNOWLEDGMENTS

We are thankful to Dr. S. Krishna Prasad, Centre for Liquid Crystal Research, Bangalore, and Professor N. V. Madhusudana, Raman Research Institute, Bangalore, for useful discussions. We are indebted to M/s Eastman Organic Chemicals for supplying, free of charge, the sample of BEPC used in this study.

-
- [1] S. Chandrasekhar, *Liquid Crystals* (Cambridge University Press, Cambridge, England, 1992), Chap. 3.
- [2] L. M. Blinov and V. G. Chigrinov, *Electrooptic Effects in Liquid Crystal Materials* (Springer, Berlin, 1994), Chap. 4.
- [3] W. Pesch and U. Behn, in *Evolution of Spontaneous Structures in Dissipative Continuous Systems*, edited by F. H. Busse and S. C. Muller (Springer, Berlin, 1998).
- [4] V. A. Delev, A. P. Krekhov, and L. Kramer, *Mol. Cryst. Liq. Cryst. Sci. Technol., Sect. A* **366**, 849 (2001).
- [5] B. Dressel, A. Joets, L. Pastur, W. Pesch, E. Plaut, and R. Ribotta, *Phys. Rev. Lett.* **88**, 024503 (2002).
- [6] B. Dressel and W. Pesch, *Phys. Rev. E* **67**, 031707 (2003).
- [7] R. Ribotta, A. Joets, and L. Lei, *Phys. Rev. Lett.* **56**, 1595 (1986).
- [8] L. Kramer, in *Pattern Formation in Liquid Crystals*, edited by A. Buka and L. Kramer (Springer, Berlin, 1996).
- [9] A. L. Munoz, T. Bock, M. Muller, W. Schopf, and I. Rehberg, *New J. Phys.* **5**, 63(1) (2003).
- [10] K. S. Krishnamurthy and M. S. Bhate, *Mol. Cryst. Liq. Cryst.* **128**, 29 (1985).
- [11] K. S. Krishnamurthy, *Mol. Cryst. Liq. Cryst.* **133**, 1 (1986).
- [12] M. C. Cross and P. C. Hohenberg, *Rev. Mod. Phys.* **65**, 851 (1993); J. P. Gollub and J. S. Langer, *ibid.* **71**, 396 (1999).
- [13] E. Moses, J. Fineberg, and V. Steinberg, *Phys. Rev. A* **35**, 2757 (1987); R. Heinrichs, G. Ahlers, and D. S. Cannell, *ibid.* **35**, R2761 (1987); P. Kolodner, *Phys. Rev. E* **50**, 2731 (1994).
- [14] S. Fauve and O. Thual, *Phys. Rev. Lett.* **64**, 282 (1990); O. Thual and S. Fauve, *J. Phys. (France)* **49**, 1829 (1988).
- [15] K. Lerman, E. Bodenschatz, D. S. Cannell, and G. Ahlers, *Phys. Rev. Lett.* **70**, 3572 (1993).
- [16] A. Joets and R. Ribotta, *Phys. Rev. Lett.* **60**, 2164 (1988); in *New Trends in Nonlinear Dynamics and Pattern-Forming Phenomena*, edited by P. Couillet and P. Huerre (Plenum Press, New York, 1990).
- [17] M. Dennin, D. S. Cannell, and G. Ahlers, *Phys. Rev. E* **57**, 638 (1998) and references therein.
- [18] U. Bisang and G. Ahlers, *Phys. Rev. E* **60**, 3910 (1999).
- [19] H. Riecke and G. D. Granzow, *Phys. Rev. Lett.* **81**, 333 (1998).
- [20] H. R. Brand, C. Fradin, P. L. Finn, W. Pesch, and P. E. Cladis, *Phys. Lett. A* **235**, 508 (1997).
- [21] W. H. de Jeu and Th. W. Lathouwers, *Mol. Cryst. Liq. Cryst.* **26**, 225 (1974); *Mol. Cryst. Liq. Cryst.* **26**, 235 (1974).
- [22] D. Balzarini and P. Palffy-Muhoray, *Liquid Crystals and Ordered Fluids*, edited by A. C. Griffin and J. F. Johnson, Vol. 4 (Plenum Press, New York, 1984), p. 531.
- [23] E. Bodenschatz, W. Zimmermann, and L. Kramer, *J. Phys. (France)* **49**, 1875 (1988).
- [24] P. A. Penz, *Phys. Rev. Lett.* **24**, 1405 (1970).
- [25] P. A. Penz, *Mol. Cryst. Liq. Cryst.* **15**, 141 (1971).
- [26] K. Kondo, A. Fukuda, and E. Kuze, *Jpn. J. Appl. Phys.* **20**, 1779 (1981).
- [27] A. Joets, A. Belaidi, and R. Ribotta, *Geometry and Topology of Caustics-Caustics 2002* (Banach Centre Pub. 62, Warsaw, 2004); E. Plaut, A. Joets, and R. Ribotta, *J. Phys. III* **7**, 2459 (1997) and references therein.
- [28] C. Mauguin, *Bull. Soc. Fr. Mineral.* **34**, 71 (1911).
- [29] N. V. Madhusudana, P. P. Karat, and S. Chandrasekhar, in *Pramana, Supplement*, edited by S. Chandrasekhar (Indian Academy of Sciences, Bangalore, 1973).
- [30] E. Plaut, W. Decker, A. G. Rossberg, L. Kramer, W. Pesch, A. Belaidi, and R. Ribotta, *Phys. Rev. Lett.* **79**, 2367 (1997).

- [31] R. Ribotta, in *Solitons in Liquid Crystals*, edited by L. Lam and J. Prost (Springer, Berlin, 1992).
- [32] A. Buka, N. Eber, W. Pesch, and L. Kramer, in *Self-Assembly, Pattern Formation and Growth Phenomena in Nanosystems*, edited by A. Golvin (Kluwer Academic Press, New York, 2005).
- [33] V. G. Chigrinov, T. V. Korkishko, M. I. Barnik, and A. N. Trufanov, *Mol. Cryst. Liq. Cryst.* **129**, 285 (1985).
- [34] H. Riecke and W. J. Rappel, *Phys. Rev. Lett.* **75**, 4035 (1995).
- [35] S. Pikin, G. Ryschenkow, and W. Urbach, *J. Phys. (France)* **37**, 241 (1976).
- [36] A. N. Trufanov, M. I. Barnik, L. M. Blinov, and V. G. Chigrinov, *Sov. Phys. JETP* **53**, 355 (1981).
- [37] P. Kolodner, *Phys. Rev. A* **44**, 6466 (1991); H. Riecke, *Phys. Rev. E* **52**, 5685 (1995).
- [38] P. B. Umbanhower, F. Melo, and H. L. Swinney, *Nature* **382**, 793 (1996); C. Crawford and H. Riecke, *Physica D* **129**, 83 (1999).
- [39] A. G. Petrov and G. Durand, *Liq. Cryst.* **17**, 543 (1994).
- [40] S. Yablonski, M. Rajteri, C. Oldano, and G. Durand, *Proc. SPIE* **2731**, 87 (1996).